Selective vulnerability of different types of commissural neurons for amyloid β-protein-induced neurodegeneration in APP23 mice correlates with dendritic tree morphology

Estibaliz Capetillo-Zarate,[1] Matthias Staufenbiel,[4] Dorothee Abramowski,[4] Christian Haass,[2] Angelika Escher,[3] Christine Stadelmann,[3] Haruyasu Yamaguchi,[5] Otmar D. Wiestler[1,*] and Dietmar Rudolf Thal[1]

[1]Department of Neuropathology, University of Bonn, Bonn, [2]Department of Biochemistry, Adolf-Butenandt Institute, Ludwig Maximilians University, Munich, [3]Department of Neuropathology, Georg-August University, Göttingen, Germany, [4]Novartis Institutes for Biomedical Research Basel, Basel, Switzerland, [5]Gunma University School of Health Sciences, Maebashi, Gunma, Japan
*Present address: DKFZ-German Cancer Research Center, D-69120 Heidelberg, Germany

Correspondence to: Dietmar R. Thal, MD, Department of Neuropathology, University of Bonn, Sigmund Freud Strasse 25, D-53105 Bonn, Germany
E-mail: Dietmar.Thal@uni-bonn.de

The amyloid β-protein (Aβ) is the main component of Alzheimer's disease-related senile plaques. Although Aβ is associated with the development of Alzheimer's disease, it has not been shown which forms of Aβ induce neurodegeneration *in vivo* and which types of neurons are vulnerable. To address these questions, we implanted DiI crystals into the left frontocentral cortex of APP23 transgenic mice overexpressing mutant human *APP* (amyloid precursor protein gene) and of littermate controls. Traced commissural neurons in layer III of the right frontocentral cortex were quantified in 3-, 5-, 11- and 15-month-old mice. Three different types of commissural neurons were traced. At 3 months of age no differences in the number of labelled commissural neurons were seen in APP23 mice compared with wild-type mice. A selective reduction of the heavily ramified type of neurons was observed in APP23 mice compared with wild-type animals at 5, 11 and 15 months of age, starting when the first Aβ-deposits occurred in the frontocentral cortex at 5 months. The other two types of commissural neurons did not show alterations at 5 and 11 months. At 15 months, the number of traced sparsely ramified pyramidal neurons was reduced in addition to that of the heavily ramified neurons in APP23 mice compared with wild-type mice. At this time Aβ-deposits were seen in the neo- and allocortex as well as in the basal ganglia and the thalamus. In summary, our results show that Aβ induces progressive degeneration of distinct types of commissural neurons. Degeneration of the most vulnerable neurons starts in parallel with the occurrence of the first fibrillar Aβ-deposits in the neocortex, that is, with the detection of aggregated Aβ. The involvement of additional neuronal subpopulations is associated with the expansion of Aβ-deposition into further brain regions. The vulnerability of different types of neurons to Aβ, thereby, is presumably related to the complexity of their dendritic morphology.

Keywords: Alzheimer's disease pathology; animal models; beta-amyloid; neurodegenerative mechanisms; selective vulnerability

Abbreviations: Aβ = amyloid β protein; APP = amyloid precursor protein; BDA = biotinylated dextran amine; ELISA = enzyme-linked immunosorbent assay; NFTs = neurofibrillary tangles; PFA = paraformaldehyde

Received February 28, 2006. Revised April 20, 2006. Accepted June 7, .2006. Advance Access publication July 14, 2006.

Introduction

Alzheimer's disease is histopathologically characterized by amyloid β-protein (Aβ) deposits and neurofibrillary tangles (NFTs) (Masters *et al.*, 1985; Braak and Braak, 1991; Dickson, 1997; Esiri *et al.*, 1997). Aβ is derived from the amyloid precursor protein (APP) (Kang *et al.*, 1987). Mutations in the *APP* gene are linked to early onset familial Alzheimer's disease (Tanzi *et al.*, 1987; Bertram and Tanzi, 2003). Transgenic mice overexpressing human *APP* harbouring these mutations are used as models for studying Alzheimer's disease-related Aβ-deposition. Aβ-deposits in humans as well as in transgenic mouse models appear predominantly in the neocortex and hippocampus (Alzheimer, 1907; Braak and Braak, 1991; Arriagada *et al.*, 1992; Games *et al.*, 1995; Hsiao *et al.*, 1996; Sturchler-Pierrat *et al.*, 1997) and expand in a similar hierarchical sequence throughout the brain (Thal *et al.*, 2002*b*; Wiederhold *et al.*, 2004; Thal *et al.*, 2006). Although synaptic changes represent an important feature of Alzheimer's disease pathology (DeKosky and Scheff, 1990; Masliah *et al.*, 1994) and Aβ-toxicity (Lacor *et al.*, 2004; Tsai *et al.*, 2004), it is not clear whether increasing levels of Aβ as represented by the hierarchical deposition of Aβ in different brain regions support the progression of neurodegeneration.

In APP-transgenic mouse models there is only minor neuronal loss (Calhoun *et al.*, 1998; Schmitz *et al.*, 2004) and no tangle formation (Games *et al.*, 1995; Masliah *et al.*, 1996; Sturchler-Pierrat *et al.*, 1997). Recently, Wu *et al.* (2004) described dendritic alterations in superficial granule cells of the dorsal blade of the dentate gyrus in young PDAPP mice. However, it is not clear whether such alterations of the dendritic tree lead to changes in neuronal connectivity.

In the human brain, pyramidal cells of the layers III and V are vulnerable to Alzheimer's disease (Alzheimer, 1907; Terry *et al.*, 1981; Braak and Braak, 1991; Duyckaerts and Dickson, 2003). Axonal loss in the corpus callosum seen in the early stages (Hampel *et al.*, 1998; Weis *et al.*, 1991; Yamauchi *et al.*, 1993) indicates that commissural neurons in these layers display an early target of Alzheimer's disease-related neurodegeneration. Furthermore, the number of neurons in layers III and V in the frontal neocortex is reduced in Down syndrome cases (Davidoff, 1928). Therefore, commissural neurons of layer III of the frontal neocortex from APP-transgenic mice represent a suitable model for studying Aβ-induced changes in neuronal connectivity.

To measure the progression of Aβ-induced neurodegeneration in commissural neurons in APP transgenic mice, we examined the degree of neuronal connectivity in layer III of the frontocentral neocortex at 3, 5, 11 and 15 months of age. To determine the degree of neuronal connectivity, retrograde tracing—a sensitive method to measure the number of neurons being connected to the tracer application site—was used. A decrease in the number of traced neurons would mean a loss of connectivity caused by several reasons such as neuronal death, axonal injury or decrease of collaterals sent from a given type of neurons.

Using this tracing method we showed that degeneration of neuronal connectivity starts in parallel with the occurrence of fibrillar Aβ-deposits, that is, aggregated Aβ, in the neocortex of 5-month-old APP23 mice and is restricted to a distinct type of neurons. Expansion of Aβ-deposition into further brain regions and the increasing Aβ-levels lead to the involvement of a second type of commissural neurons.

Material and methods

Animals

APP23 mice were generated as described previously (Sturchler-Pierrat *et al.*, 1997) and continuously back-crossed to C57BL/6. An expression construct containing a murine Thy-1 promoter was used to drive neuron-specific expression of human mutant APP751 with the Swedish double mutation 670/671 KM→NL. Heterozygous female APP23 mice were analysed at 3 months of age ($n = 12$), 5 months of age ($n = 16$), 11 months of age ($n = 13$) and 15 months of age ($n = 15$). As control, female wild-type littermates were analysed at 3 months of age ($n = 8$), 5 months of age ($n = 13$), 11 months of age ($n = 14$) and 15 months of age ($n = 9$).

Brain homogenates, immunoprecipitation, western blot analysis and enzyme-linked immunosorbent assay (ELISA)

Forebrain hemispheres (excluding olfactory bulb, cerebellum and brainstem) were weighed and homogenized by sonication in 10 vol. of buffer [20 mM Tris–HCl (pH 7.6), 137 mM sodium chloride, protease inhibitor cocktail (Complete, Roche Molecular Biochemical, Mannheim, Germany)]. For immunoprecipitation, homogenates were supplemented with 1% sodium dodecyl sulphate, heated to 95°C for 3 min, diluted with 9 vol. of homogenization buffer and cleared by centrifugation at 15°C for 15 min at $20\,000\times g$. Aβ-peptides were immunoprecipitated using the monoclonal antibody β1 reacting with the amino-terminus of Aβ (Schrader-Fischer and Paganetti, 1996) and protein G-coated magnetic beads (Dynal Biotech, Hamburg, Germany). Precipitates or whole homogenates were separated on 10% Tris–bicine gels with 8 M urea as described (Klafki *et al.*, 1996; Staufenbiel and Paganetti, 1999). In this system, Aβ$_{1–40}$ migrates slower than Aβ$_{1–42}$. Proteins were transferred to Immobilon-P membranes (Millipore, Carrigtwohill, Ireland). Aβ-peptides were fixed to the membrane by heating it to 95°C for 3 min in phosphate-buffered saline (PBS; Sigma, Taufkirchen, Germany) (Staufenbiel and Paganetti, 1999). Full-length APP (flAPP) was detected with rabbit antiserum APP-C8 raised against the carboxy-terminal amino acids of APP (Schrader-Fischer and Paganetti, 1996), which are identical in mice and humans. Transgene-derived APP and Aβ were detected with the monoclonal antibody 6E10 (Signet, MA, USA). After incubation of the blots with the appropriate peroxidase coupled secondary antibodies (Jackson Immunoresearch, Soham, UK and Sigma, Taufkirchen, Germany), proteins were detected by visualizing chemiluminescence (ECL advance, Amersham Pharmacia Biotech, NJ, USA) on autoradiographic films (Hyperfilm ECL, Amersham Pharmacia Biotech).

For analysis of Aβ by ELISA, forebrain homogenates from APP23 mice of each age group (3 months: $n = 6$; 5 months: $n = 6$; 11 months: $n = 4$; 15 months: $n = 7$) were supplemented with concentrated

formic acid to a final concentration of 70%. After 15 min of incubation on ice and mixing every 5 min, the samples were neutralized by addition of 19 vol. 1 M Tris base supplemented with protease inhibitor cocktail. The extracts were cleared by centrifugation (20 000× *g* for 15 min at 4°C). Supernatants from young (3 or 5 months) APP23 mice were directly loaded on sandwich ELISA plates for quantification of Aβ-peptides (Aβ$_{1-40}$: ELISA from IBL, Hamburg, Germany; Aβ$_{1-42}$: ELISA from Innogenetics, Ghent, Belgium). Supernatants from 11- and 15-month-old APP23 mice were diluted as necessary in dilution buffers supplied with the ELISAs. Standard curves were prepared with synthetic peptides Aβ$_{1-40}$ and Aβ$_{1-42}$ purchased from Bachem (Bubendorf, Switzerland) and diluted in extracts of non-transgenic mouse forebrain prepared in parallel as described above. Each sample was analysed in duplicate.

Tissue preparation and DiI tracing

For DiI tracing brains of 3-, 5-, 11- and 15-month-old APP23 (3 months: *n* = 6; 5 months: *n* = 9; 11 months: *n* = 8; 15 months: *n* = 8) and wild-type mice (3 months: *n* = 6; 5 months: *n* = 12; 11 months: *n* = 13; 15 months: *n* = 9) were studied. Animals were treated in agreement with the German law on the use of laboratory animals. Mice were anaesthetized. Perfusion was performed transcardially with Tris-buffered saline (TBS) with heparin (pH 7.4) followed by the injection of 0.1 M PBS (pH 7.4) containing 2.6% paraformaldehyde (PFA), 0.8% iodoacetic acid, 0.8% sodium periodate and 0.1 M D-L lysine. The brains were removed in total and post-fixed in 2.6% phosphate-buffered PFA (pH 7.4) containing 0.8% iodoacetic acid, 0.8% sodium periodate and 0.1 M D-L lysine (Galuske *et al.*, 2000). Three days later a single crystal (∼0.3 mm³) of the carbocyanine dye DiI (Molecular Probes, Eugene, OR, USA) was implanted into the left frontocentral cortex, 1 mm rostrally from the central sulcus, 2 mm laterally from the middle line and 1 mm deep in the cortex (Fig. 1A). This dye allows precise Golgi-like tracing of neurons in post-mortem fixed tissue in a quality similar to *in vivo*

tracing methods using rhodamine tracers even in only weakly traced neurons (Galuske and Singer, 1996). After incubation in 2.6% phosphate-buffered PFA for at least 3 months at 37°C, 100-μm-thick coronal vibratome sections were cut. Sections were mounted in TBS for microscopic analysis.

In vivo tracing with biotinylated dextrane amine (BDA)

For *in vivo* tracing with BDA (Molecular Probes), three 3-month-old C57BL/6 wild-type mice were anaesthetized with ketamine/Rompun and placed in a stereotactic frame. After incision of the skin, a fine hole was drilled into the skull 0.1 mm caudal and 0.2 mm lateral to bregma. A finely drawn glass capillary was stereotactically placed into the frontal cortex (approximal depth = 0.5 mm), and 1 μl BDA was slowly injected over a 3-min period. After withdrawal of the capillary, the skin wound was closed by suture, and animals were allowed to survive for 3 days. For tissue sampling, animals were anaesthetized, perfused transcardially with 4% PFA and dissected. Brain slices were embedded in gloop, a mixture of egg albumin, gelatine, sucrose and glutaraldehyde, and 50-μm vibratome sections were cut. BDA was visualized using an avidin–peroxidase-based method (Vectastain, Vector Laboratories, Burlingame, CA, USA) with 3,3-diaminobenzidine (DAB) as chromogen. Sections were dehydrated and coverslipped.

Microscopic and quantitative analysis

In layer III of the frontocentral cortex of the right hemisphere, contralateral to the implantation site of the tracer, the morphology of traced commissural neurons was examined. The traced neurons were assigned to different types according to their morphology. Then the number of traced commissural neurons of each type in wild-type mice was compared with that in APP23 mice. For qualitative and quantitative analysis 10 consecutive sections (100-μm
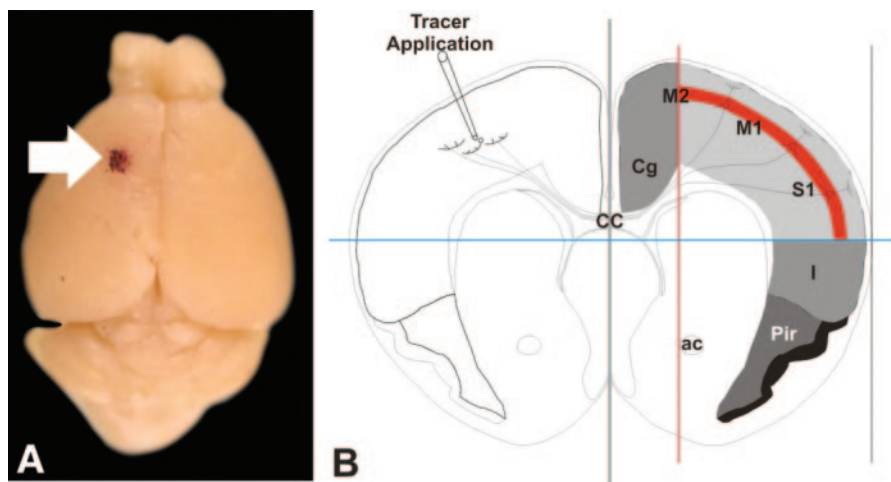
Fig. 1 Application site of the DiI tracer in the mouse brain and region of interest for the analysis of traced commissural neurons. (**A**) The DiI tracer was implanted into the left frontocentral cortex: 1 mm rostrally from the central sulcus, 2 mm laterally from the median sagittal plane and 1 mm deep in the cortex (arrow). In so doing, the tracer was placed into layers I–V of the frontocentral cortex. (**B**) The schematic representation shows a coronal section of the mouse brain at the level of the tracer application site. Layer III commissural neurons within the contralateral frontocentral cortex labelled by the DiI tracer were studied in the secondary and primary motor cortex (M1 and M2) and the somatosensory cortex (S1) (area marked in red) as determined by the following coordinates: the medial boundary was established as the vertical (red) line that separates the cingulate cortex (Cg) from the secondary motor cortex (M2). The horizontal limit was referred to as the horizontal (blue) line that separated the primary somatosensory cortex (S1) from the insular cortex (I).

thickness each) representing a tissue block of 1 mm thickness were studied for each mouse. Analysis started at the anterior commissure setting the caudal limit of the investigated tissue block. For each coronal section, the medial boundary of the region investigated was set as the vertical line at the cingulum that separated the cingulate cortex (Cg) from secondary motor cortex (M2) (Fig. 1B). The horizontal boundary was set as the horizontal line separating the primary somatosensory cortex (S1) from the insular cortex (I) (Fig. 1B).

For the qualitative analysis a laser scanning confocal microscope (Leica TCS NT, Leica, Bensheim, Germany) was used. Stacks of 2D images were superimposed digitally using the Image J Image Processing and Analysis software (NIH, Bethesda, MD, USA), and 3D data sets were generated for the visualization of neurons with their entire dendritic tree.

For quantification of the commissural neurons in APP-transgenic and wild-type mice, traced neurons in layer III were counted in the region of interest depicted in Fig. 1 in 10 consecutive sections of the tissue block taken for qualitative and quantitative analysis using a fluorescence microscope (Leica DMLB, Leica). In so doing, we analysed a cortex volume of 5–6 mm^3 in each mouse. Mean and median values of the number of traced neurons were calculated and compared between wild-type and APP23 mice. Statistical analysis was performed using the Mann–Whitney U-test to compare wild-type and APP23 mice. Poisson regression was used to identify differences among the different phases of Aβ-deposition in the brain. Appropriate corrections for multiple testing were made. SPSS 11.0 (SPSS, Chicago, IL, USA) and LogXact 5.0 (Cytel Software Corporation, Cambridge, MA, USA) software were used to calculate statistical tests.

Immunohistochemistry

Immunohistochemistry was performed for the detection and quantification of Aβ-plaques. After formic acid pretreatment free-floating sections were incubated with an anti-Aβ antibody [polyclonal rabbit (Wild-Bode *et al.*, 1997), 1/750, 24 h at 22°C]. The polyclonal antibody detected Aβ$_{1-40}$ as well as Aβ$_{1-42}$. To separately detect Aβ$_{40}$ and Aβ$_{42}$ positive material, additional sections were stained with monoclonal antibodies specifically detecting the C-terminus of Aβ$_{40}$ [MBC40 (Yamaguchi *et al.*, 1998), 1/20, 24 h at 22°C, formic acid pretreatment] and Aβ$_{42}$ [MBC42 (Yamaguchi *et al.*, 1998), 1/200, 24 h at 22°C, formic acid pretreatment]. The primary antibody was detected with a biotinylated secondary antibody and the ABC complex, and visualized with DAB (Hsu *et al.*, 1981). Sections were mounted in Corbit® (Hecht, Hamburg, Germany).

Quantification of the Aβ-plaque load was performed in an area of the frontocentral neocortex in one selected section with plaques using a Zeiss Stemi2000C microscope and Axiovision AC 4.2 image analysis software (Carl Zeiss Lichtmikroskopie, Göttingen, Germany). The Aβ-plaque load was measured for plaques stained with the polyclonal antibody raised against Aβ$_{1-42}$ (Wild-Bode *et al.*, 1997) according to the following determination:

$$\text{Aβ-plaque load} = \frac{\text{area of plaques detected with anti-Aβ}_{1-42} \text{ antibodies in a given region of interest} \times 100}{\text{area of the region of interest}}$$

Mean values of the Aβ-plaque load were compared between 3-, 5-, 11- and 15-month-old APP23 mice with ANOVA (analysis of variance).

To characterize the expansion of Aβ-deposition in the mouse brain we determined the phases of Aβ-deposition valid for

Table 1 Phases of Aβ-deposition in APP23 mice brain

|	
Phase 0	Absence of Aβ deposits
Phase 1	Aβ deposits in the neocortex
Phase 2	Aβ deposits in the neocortex and allocortex
Phase 3	Aβ deposits in the neocortex, allocortex, thalamus and striatum
Phase 4	Aβ deposits in the neocortex, allocortex, thalamus, striatum and midbrain basal ganglia and brainstem
Phase 5	Aβ deposits in the neocortex, allocortex, thalamus, striatum, brain stem and cerebellum

human and APP-transgenic mouse brain (Thal *et al.*, 2002*b*; Wiederhold *et al.*, 2004; Thal *et al.*, 2006) (Table 1).

To identify axonal sprouting and axonal damage, sections of the area of interest of each mouse were stained with antibodies directed against APP (22C11, monoclonal mouse, Chemicon (Temecula, CA, USA), 1/75, 24 h at 22°C) and against growth-associated protein GAP43 (polyclonal rabbit, Chemicon, 1/75, 24 h at 22°C) (Masliah *et al.*, 1992*a*, *b*).

Results
Subpopulations of commissural neurons in layer III of the frontocentral cortex

Using retrograde tracing with DiI, three different types of commissural neurons were identified in layer III of the frontocentral cortex in wild-type and APP23 mice at the age of 3, 5, 11 and 15 months (Fig. 2A–F). The first type of commissural neurons, referred to as type I, showed a DiI-labelled perikaryon of pyramidal shape, an apical dendrite and multiple basal dendrites with a heavily ramified and spiny dendritic tree. Ramification of the dendrites was characterized by branching of apical and basal dendrites into primary branches exhibiting secondary and tertiary ramifications within layer III (Fig. 2A and D). The basal dendrites were restricted to layers II/III. The apical dendrite showed further ramification within the molecular layer. These type I commissural neurons were predominantly located in the upper part of layer III (Fig. 2D). The second type of commissural neurons, referred to as type II, exhibited a DiI-labelled perikaryon of pyramidal shape. The apical and basal dendrites were detectable, but further ramification and dendritic spines were less frequently observed and the basal dendrites were thicker than those of type I commissural neurons (Fig. 2B, E and F). 3D reconstruction revealed that the basal dendrites of type II commissural neurons start branching distant from the perikaryon (Fig. 2F). Commissural neurons of type II showed dendritic ramification and spines in the molecular layer as detected by following the apical dendrite in consecutive sections and, thus, represent the classical pyramidal cell morphology. These neurons were most frequently located in the lower part of layer III. Branches of their basal dendrites were also seen in the upper part of layer IV (Fig. 2E and F). The third type of commissural neurons, referred to as type III, did not exhibit clearly distinguishable apical and basal dendrites within layer III.
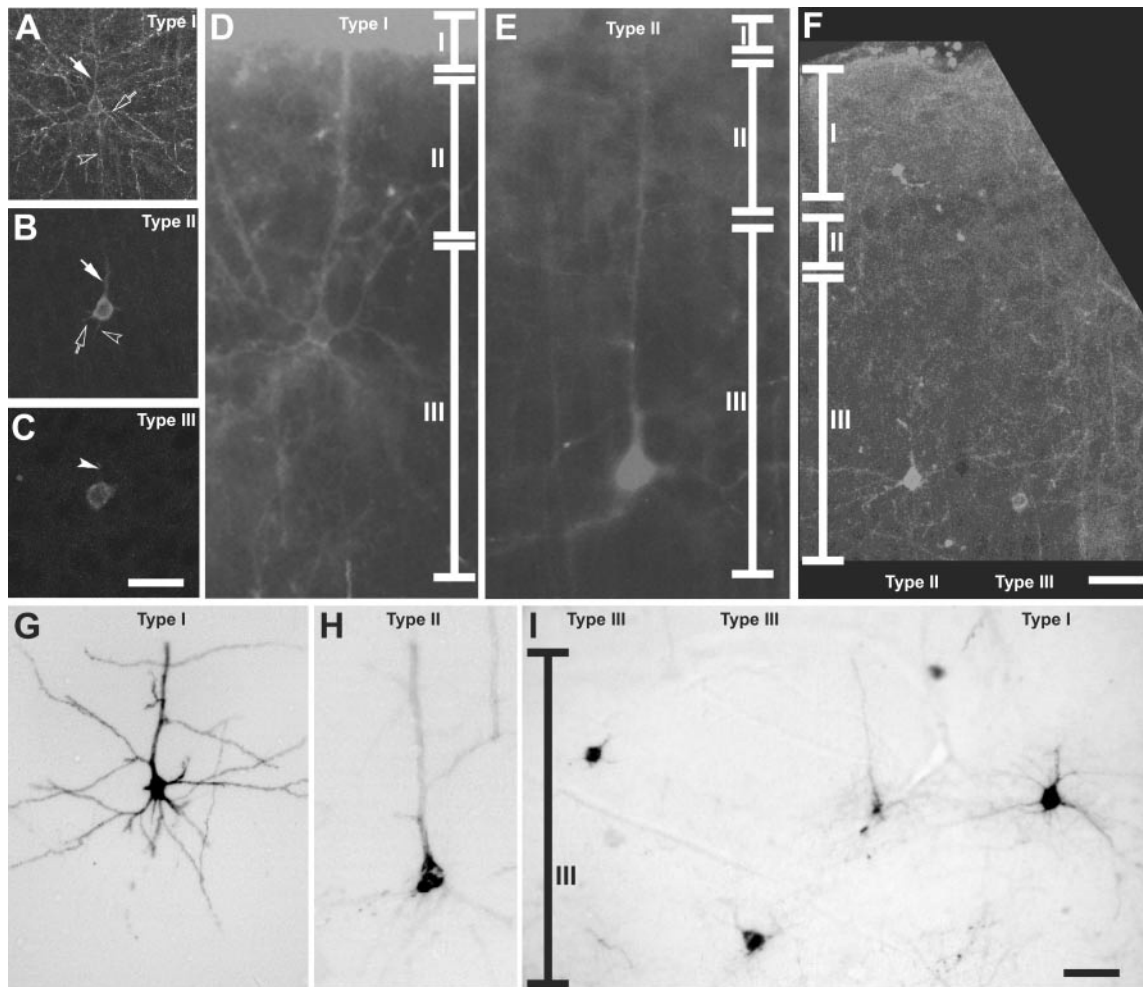
Fig. 2 Three types of commissural neurons traced in the frontocentral cortex of wild-type mice. **A**, **B** and **C** show the typical pattern of these three types of neurons as characterized in 100-μm-thick sections after tracing with DiI. Type I commissural neurons are characterized as pyramidal shaped neurons with apical (white arrow) and basal (unfilled arrow) dendrites creating a heavily ramified and spiny dendritic tree showing secondary and tertiary branches within layer III. The axon leaves the perikaryon at the base (unfilled arrowhead; **A**). These neurons are mainly located within the upper part of layer III (**D**). The second type of commissural neurons is the sparsely ramified pyramidal neuron. These neurons are also characterized by a pyramidal cell body and traced apical (white arrow) and basal (unfilled arrow) dendrites. These cells represent the classical pyramidal cells in layer III. There is almost no further ramification of the apical and basal dendrite detectable in this type of neuron within layer III. The basal dendrites start branching distant from the perikaryon as shown in a 3D reconstruction of serial scans (**F**). The axon is visible at the base of the perikaryon (unfilled arrowhead; **B**). These neurons are preferentially found in the lower part of layer III (**E** and **F**). (**C**) Non-pyramidal commissural neurons, referred to as type III commissural neurons, are characterized by a circular cell body. A few dendrites arise from the perikaryon (arrowhead). There is no further ramification seen in this type of neuron. The axon is not seen in this section. Type III commissural neurons do not exhibit a distinct predilection site within layer III (**F** and **I**). (**G–I**) Tracing with biotinylated dextran confirms the staining pattern of the three types of commissural neurons as seen with DiI tracing. **A–C** show DiI-traced neurons in wild-type mice at 11 months of age, **D–F** in those of 5 months of age. **A–C** and **F** represent 3D stacks of 16 images of cells 1.25–1.75 μm distance recorded with the laser scan confocal microscope; **D** and **E** are images digitally captured with the Leica DMLB-microscope. (**G–I**) Commissural neurons traced with biotinylated dextran 3 days before death in wild-type mice of 3 months of age mice. Calibration bar in **C** valid for **A**: 55 μm, **B** and **C**: 40 μm. Calibration bar in **F** valid for **D** and **E**: 35 μm, **F**: 50 μm. Calibration bar in **I** valid for **G–I**: 35 μm.

Only the cell body with a circular shape was clearly labelled with the tracer. Single, very thin dendrites without spines were labelled in layer III (Fig. 2C and F). These neurons did not show a predilection site in layer III. They occurred in the upper as well as in the lower parts of this cell layer. In all types of commissural neurons the axon left the neuron at the base and was part of the callosal commissural fibre system. *In vivo* tracing of wild-type mice with BDA confirmed the staining pattern and the existence of three different types of commissural neurons seen in the DiI-traced sections (Fig. 2G–I).

Alteration of commissural neurons in APP23 mice

At 3 months of age there were no differences between wild-type and APP23 mice in the morphology of the commissural
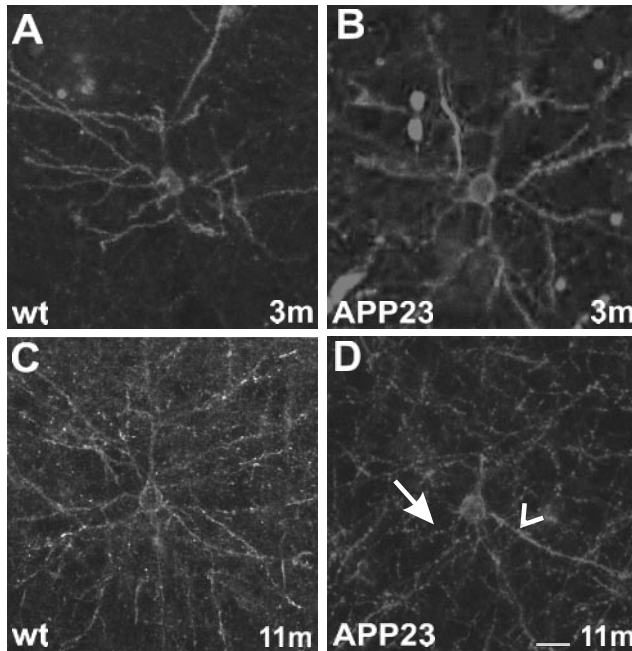
Fig. 3 DiI-traced type I commissural neurons in the frontocentral cortex of 3- and 5-month-old wild-type and APP23 mice. (**A**) Type I commissural neurons in layer III of the frontocentral cortex show a highly ramified dendritic tree in 3-month-old wild-type mice. The basal dendrites exhibit secondary and tertiary branches and are symmetrically organized. (**B**) In APP23 mice of 3 months of age there are no significant differences in the architecture of the dendritic tree when compared with that of wild-type animals. (**C**) In 11-month-old wild-type animals the dendritic tree of a type I commissural neuron shows further ramifications. The dendritic tree has still a perfect symmetric architecture. (**D**) Type I commissural neuron in an 11-month-old APP23 mouse exhibits a dendritic tree that shows a non-symmetric architecture of the basal dendrites. A number of basal dendrites are small and shrunken (arrow) while others still appear in regular size (unfilled arrowhead). This pattern of type I neurons is strikingly different from that at 3 months of age and that of wild-type animals at 11 months of age. Calibration bar: 22 μm.

neurons (Fig. 3A and B). In contrast, type I commissural neurons were morphologically altered in APP23 mice compared with wild-type mice at 5, 11 and 15 months of age (Fig. 3C and D). In APP23 mice, the apical dendrite was shorter than that in wild-type animals (Fig. 3C and D). The basal dendrites exhibited a non-symmetric pattern and short secondary or tertiary branches, and their diameter was often reduced (Fig. 3D). In comparison, in wild-type mice this type of neurons showed a symmetrical architecture of the basal dendrites and secondary and tertiary branches were longer than those in APP23 transgenic mice (Fig. 3C and D). Altered type I commissural neurons in APP23 mice were often located distant from Aβ-plaques identified by subsequent immunostaining with anti-Aβ$_{1-42}$ or by Aβ-plaque-induced autofluorescence (Thal *et al.*, 2002*a*).

There were no apparent differences in the morphological patterns of type II and type III commissural neurons among APP23 and wild-type mice.

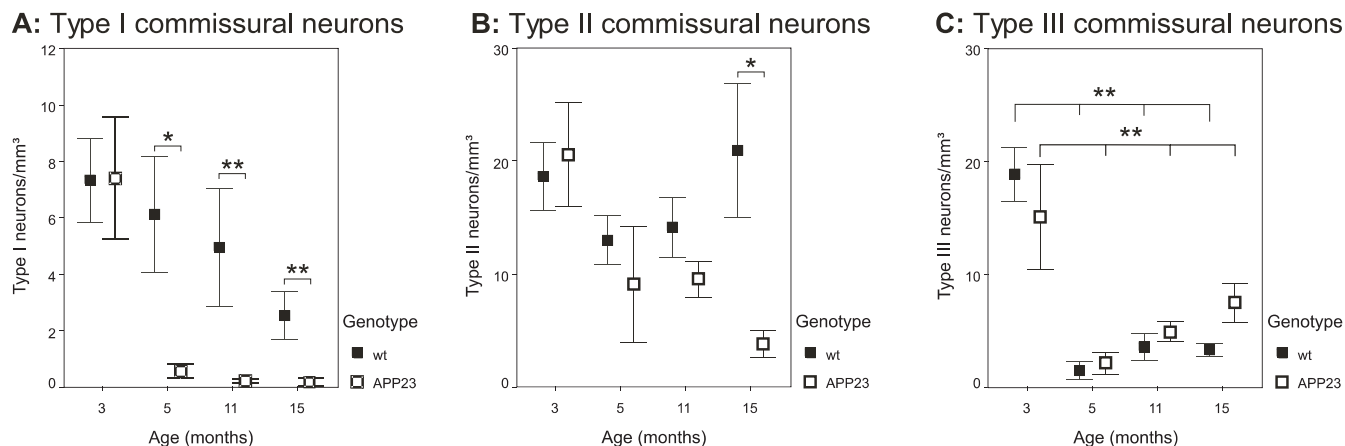## Selective reduction of type I commissural neurons in APP23 mice

Quantitative analysis of traced commissural neurons in 5- to 15-month-old wild-type mice showed that type II commissural neurons were predominant (60–80%), while type I (10–20%) and type III neurons (10–20%) were less abundant. The number of traced type I neurons appeared to decrease with age, but this trend failed significance (trend test: $P = 0.108$) (Fig. 4A). In 3-month-old animals a similar percentage of type I neurons was found (10–20%) while type II neurons were less predominant (40–45%). In these animals the number of type III neurons was higher than that in older animals ($P < 0.01$; ANOVA corrected for multiple testing by using the Tamhane T2 *post hoc* test) and covered 40–45% of all traced commissural neurons (Fig. 4C).

The overall number of commissural neurons did not show significant differences between wild-type and transgenic mice at a given age (Mann–Whitney U-test, corrected for multiple testing: 3 months: $P = 0.9917$; 5 months: $P = 0.2126$; 11 months: $P = 0.9579$; 15 months: $P = 0.3232$). However, with increasing expansion of Aβ-deposition throughout the brain the total number of neurons decreased (Poisson regression analysis controlled for age: risk-ratio = 0.967, 95% confidence interval (CI) = 0.941–0.9938, $P < 0.05$; trend-test: $P < 0.05$).

In detail, the number of traced type I commissural neurons in APP23 mice was reduced by >90% compared with that of wild-type mice at 5, 11 and 15 months of age (Mann–Whitney U-test, corrected for multiple testing: 5 months APP23 versus wild-type: $P < 0.05$; 11 months APP23 versus wild-type: $P < 0.005$; 15 months APP23 versus wild-type: $P < 0.01$) but not at 3 months of age (Mann–Whitney U-test, corrected for multiple testing: 3 months APP23 versus wild-type: $P = 0.9917$) (Fig. 4A). With the expansion of Aβ-deposition the number of traced type I neurons decreased significantly (Poisson regression analysis controlled for age: risk-ratio = 0.3417, CI = 0.174 − 0.6712, $P < 0.005$).

The number of type II commissural neurons did not show significant differences between wild-type and APP23 mice at 3, 5 and 11 months of age (Mann–Whitney U-test, corrected for multiple testing: 3 months: $P = 1$; 5 months: $P = 0.182$; 11 months: $P = 0.9375$) (Fig. 4B). However, at 15 months of age a significant reduction of traced type II neurons was observed in APP23 mice compared with wild-type (Mann–Whitney U-test, P-values corrected for multiple testing: 15 months: $P < 0.05$). Over all ages the number of traced type II neurons decreased significantly with the expansion of Aβ-deposition (Poisson regression analysis controlled for age: risk-ratio = 0.9432, CI = 0.9033–0.9849, $P < 0.01$).

The number of type III commissural neurons did not significantly differ among APP23 and wild-type mice, neither at 3 nor at 5, 11 or 15 months of age (Mann–Whitney U-test, corrected for multiple testing: APP23 versus

A: Type I commissural neurons

B: Type II commissural neurons


C: Type III commissural neurons

Fig. 4 Diagrams representing mean number and standard deviation of type I, II and III commissural neurons in each strain at 3, 5, 11 and 15 months of age. (**A**) Type I commissural neurons in wild-type and APP23 mice at 3, 5, 11 and 15 months of age. APP23 mice show a decrease of >90% of the type I commissural neurons compared with wild-type mice at 5, 11 and 15 months of age. (**B**) Type II commissural neurons in wild-type and APP23 mice. There are no significant differences in the number of type II commissural neurons at 3, 5 and 11 months of age between wild-type and APP23 mice. Only in 15-month-old APP23 mice the number of type II commissural neurons is decreased compared with wild-type animals. At this age less type II neurons are labelled when compared with younger APP23 mice (Kruskal–Wallis *H*-test: $P < 0.005$, trend-test: $P < 0.05$). (**C**) Type III commissural neurons in wild-type and APP23 mice. Neither at 3 nor at 5, 11 and 15 months of age are there significant differences in the number of non-pyramidal commissural neurons between wild-type and APP23 mice. Between 3 months of age and 5–15 months of age there is a reduction of ~80% of type III neurons. In mice older than 3 months, type II commissural neurons are the predominant type of commissural neurons in the frontocentral cortex representing 60–80% of them. Type I and III commissural neurons are less frequently detectable than type II commissural neurons, and each represent 10–20% of the commissural neurons. *$P < 0.05$; **$P < 0.01$.

wild-type: 3 months: $P = 0.8651$; 5 months: $P = 0.9749$; 11 months: $P = 0.453$; 15 months: $P = 0.3232$) (Fig. 4C). In addition, there was no significant change in the number of traced type III neurons throughout the phases of Aβ-deposition (Poisson regression analysis controlled for age: risk-ratio = 1.0409, $P = 0.1533$).

Aβ-production and Aβ-deposition in APP23 mice

Western blot analysis confirmed overexpression of human APP and production of $A\beta_{1-40}$ and $A\beta_{1-42}$ in APP23 mice (Fig. 5). Quantification of total Aβ levels by ELISA in APP23 mice at 3, 5, 11 and 15 months of age showed a significant exponential increase of Aβ with the age (Table 2) (ANOVA corrected for multiple testing by using the Tamhane T2 *post hoc* test: $A\beta_{1-40}$ $P < 0.001$; $A\beta_{1-42}$ $P < 0.001$). Total $A\beta_{1-40}$ levels, thereby, were higher than total $A\beta_{1-42}$ levels (sign test: $P < 0.001$). Between 3 and 5 months of age total Aβ levels did not differ significantly (ANOVA corrected for multiple testing by using the Tamhane T2 *post hoc* test: $A\beta_{1-40}$ $P = 0.786$; $A\beta_{1-42}$ $P = 0.963$). However, between 5 and 11 months of age an increase of both $A\beta_{1-40}$ and $A\beta_{1-42}$ was seen (ANOVA corrected for multiple testing by using the Tamhane T2 *post hoc* test: $A\beta_{1-40}$ $P < 0.05$; $A\beta_{1-42}$ $P < 0.01$), as well as between 11 and 15 months of age (ANOVA corrected for multiple testing by using the Tamhane T2 *post hoc* test: $A\beta_{1-40}$ $P < 0.01$; $A\beta_{1-42}$ $P < 0.001$).

Immunohistochemistry with a polyclonal antibody detecting $A\beta_{1-40}$ as well as $A\beta_{1-42}$ revealed no Aβ-deposits
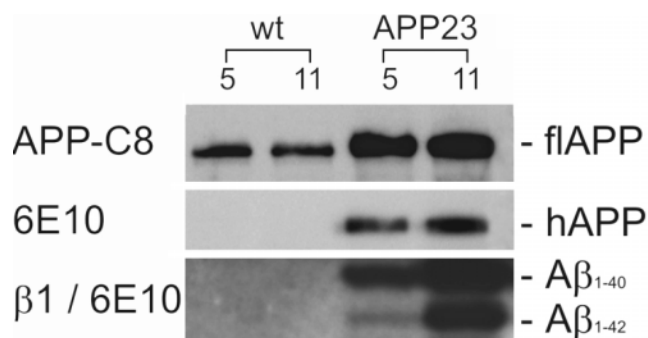
Fig. 5 Western blot analysis of APP and Aβ in forebrain homogenates of wild-type and APP23 mice at the ages of 5 and 11 months. flAPP is detected with an antibody directed against mouse and human APP (APP-C8). Transgenic human APP (hAPP) is stained with a human-specific Aβ antibody that also reacts with human APP (6E10). In the lowest panel, $A\beta_{1-40}$ and $A\beta_{1-42}$ are detected with the 6E10 antibody after immunoprecipitation with the anti-Aβ antibody β1 except for the 11-month-old APP23 sample. To compensate for the Aβ accumulation, this sample was diluted and represents 80 times less forebrain tissue than the other samples. Both $A\beta_{1-40}$ and $A\beta_{1-42}$ are detectable in APP23 mice at 5 and 11 months of age while no significant amounts of Aβ are seen in wild-type mice.

in wild-type mice at 3, 5, 11 or 15 months. APP23 mice did not show plaques at 3 months of age. Single plaques in the frontocentral neocortex were observed in 67% of the APP23 mice at 5 months of age representing Phase 1 of Aβ-deposition (Table 3) (ANOVA corrected for multiple testing by using the Tamhane T2 *post hoc* test: $P < 0.05$). However,

Table 2 Mean levels of Aβ$_{1-40}$ and Aβ$_{1-42}$ concentration in the forebrain of APP23 mice determined by ELISA

Age (months)	Aβ$_{1-40}$ (pmol/g)	SD		Aβ$_{1-42}$ (pmol/g)	SD	
3	22.51	±3.16		2.25	±0.36	
5	25.94	±5.60	} $P < 0.05$	2.46	±0.40	} $P < 0.01$
11	5447.09	±1437.67	}	1668.36	±256.46	}
15	28919.74	±7699.72	} $P < 0.01$	6019.74	±1146.88	} $P < 0.001$

Table 3 Percentage of mice exhibiting Aβ-deposits in a given phase at a given age. Animals at 15 months of age did not show higher phases than Phase 3.

Age (months)	Phase 0	Phase 1	Phase 2	Phase 3
3	100.0%	0.0%	0.0%	0.0%
5	33.3%	66.7%	0.0%	0.0%
11	0.0%	33.3%	66.7%	0.0%
15	0.0%	0.0%	11.1%	88.9%

differences in the Aβ-plaque load did not reach significance between 3- and 5-month-old APP23 mice (ANOVA corrected for multiple testing by using the Tamhane T2 *post hoc* test: $P = 0.096$) (Fig. 6A). Between 5- and 11-month-old APP23 mice the Aβ-plaque load in the frontocentral cortex increased (ANOVA corrected for multiple testing by using the Tamhane T2 *post hoc* test: $P < 0.005$). Additionally, 11-month-old mice often exhibited an involvement of allocortical brain regions, that is, the hippocampal formation and the cingulate gyrus in Aβ-deposition representing Phase 2 of Aβ-deposition (Fig. 6B, Table 3) (ANOVA corrected for multiple testing by using the Tamhane T2 *post hoc* test: $P < 0.005$). Between the ages of 11 and 15 months there was a further increase in the Aβ-plaque load within the frontocentral cortex (ANOVA corrected for multiple testing by using the Tamhane T2 *post hoc* test: $P < 0.001$) (Fig. 6A), and additional Aβ-plaques occurred in the basal ganglia as well as in the thalamus, indicating Phase 3 of Aβ-deposition (ANOVA corrected for multiple testing by using the Tamhane T2 *post hoc* test: $P < 0.001$) (Fig. 6B, Table 3). Aβ-deposits in APP23 mice exhibited equal staining patterns with anti-Aβ$_{42}$ and anti-Aβ$_{40}$ antibodies. Aβ-deposition according to the pattern of Phase 4 or Phase 5 has not been observed in 3-, 5-, 11- and 15-month-old APP23 mice.

Axonal sprouting of commissural neurons in APP23 mice

Immunohistochemistry with antibodies directed against APP and GAP43 showed the presence of immunolabelled, thickened axon endings in the frontocentral cortex of 3-month-old wild-type and APP23 mice indicative for axonal sprouting (Fig. 7A–D). In the DiI-traced sections we found collateral sprouting in wild-type and APP23 mice at 3 months of age. Single axons of commissural neurons with growth cones were seen in layers II and III of the frontocentral cortex of the DiI-traced sections (Fig. 7E). In 5-month-old mice thickened axon endings of commissural neurons in DiI-traced sections

were no longer observed. However, single APP and GAP43-positive, thickened axon endings were found in APP23 mice but not in wild-type mice at this age (Fig. 7F–I). Sprouting of commissural neurons around plaques was observed in 11- and 15-month-old APP23 mice in DiI-traced sections (Fig. 7L) as well as in APP and GAP43-stained sections (Fig. 7J and K). Wild-type mice did not show sprouting of commissural neurons in this age in DiI-traced sections. Only single APP and GAP43-positive sprouting axons were detected in the frontocentral cortex of 15-month-old wild-type mice.

Discussion

In this study, we show that three types of commissural neurons in layer III of the mouse frontocentral cortex can be identified using tracing methods. These different neuron types are hierarchically affected by Aβ-induced neurodegeneration. The deposition of the first Aβ-plaques is associated with the onset of neurodegeneration in APP23 mice. Expansion of Aβ-deposition into further brain regions goes along with the involvement of a second type of commissural neurons in neurodegeneration. The complexity of the dendritic morphology is, thereby, related to the vulnerability of these different types of neurons.

Characterization of three types of commissural neurons in the mouse frontocentral neocortex

Our study confirms and extends previous reports that describe different types of pyramidal and non-pyramidal neurons projecting through the corpus callosum (Hughes and Peters, 1992; Martinez-Garcia *et al.*, 1994). The distinction of the three types of commissural neurons in the mouse frontocentral cortex is based on their morphological appearance after retrograde tracing with DiI. It is confirmed by using biotinylated dextran *in vivo* tracing as an additional method.

Type I commissural neurons are characterized by a pyramidally shaped perikaryon and apical and basal dendrites with a heavily ramified and spiny dendritic tree within layer II–III. Type II commissural neurons represent neurons with a pyramidally shaped perikaryon and apical and basal dendrites, which do not show extensive further ramifications in layer III in a given tissue section. However, 3D reconstruction revealed that the basal dendrites of these neurons start branching distant from the perikaryon. Type III commissural
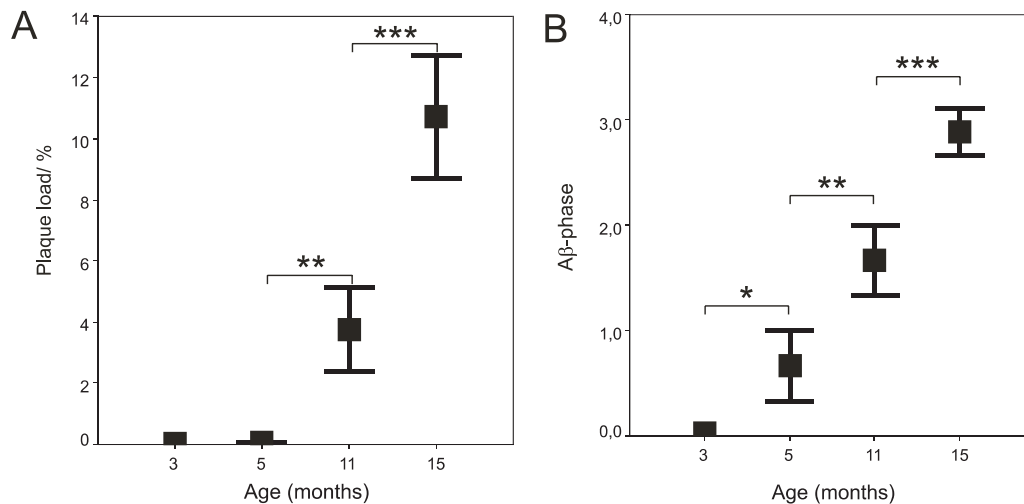
Fig. 6 (**A**) Quantification of the Aβ-plaque load in the frontocentral cortex of APP23 mice. (**A**) There is no significant difference in the Aβ-plaque load between 3- and 5-month-old animals. The single plaques seen in 5-month-old animals did not lead to a significant increase in the Aβ-plaques load ($P = 0.096$). Between 5 and 11 as well as between 11 and 15 months the Aβ-plaque load increases. (**B**) Distribution of Aβ-plaques as described by the phases of Aβ-deposition (Thal *et al.*, 2002*b*) in APP23 mice. Three-month-old animals do not show plaques. Aβ-deposition starts with the first plaques in 5-month-old APP23 mice. Sixty-seven per cent of these mice exhibited Aβ-plaques in a distribution pattern related to Phase 1. A significant expansion of Aβ-deposition as represented by an increasing phase is seen with advancing age. Boxes represent mean values. Bars indicate the standard deviation. *$P < 0.05$; **$P < 0.01$; ***$P < 0.001$.

neurons are non-pyramidal neurons and have a circular cell body with a few dendrites.

In contrast to the other types of commissural neurons, type III neurons are reduced in number in 5-, 11- and 15-month-old animals in comparison with 3-month-old mice regardless of the genotype. Thus, an effect of Aβ or APP-overexpression is not responsible for the reduction of type III neurons because wild-type mice show the same effects as APP23 mice. To explain this finding, further studies are required. Developmental or maturation-related phenomena (Fritzsch *et al.*, 1997) might be involved.

All three types of neurons were found in all mice studied, and their axons projected through the corpus callosum to the contralateral hemisphere. Since tracer-labelled type I, II and III commissural neurons were visible in the same section close to one another and type II neurons showed dendritic ramification in the molecular layer, it seems unlikely that DiI tracing of neurons without a ramified dendritic tree is due to dysfunctional tracing rather than to the exhibition of specific morphological types of neurons. Galuske and Singer (1996) also reported that in the event that a given cell is stained by DiI all cell processes will be labelled. Moreover, a second tracing method based on *in vivo* transport of the biotinylated dextrane (Reiner *et al.*, 2000) confirmed the presence of three different types of commissural neurons.

The heterogeneous morphological pattern of commissural neurons in the frontocentral cortex of mice confirms and extends the finding of other authors that the visual cortex contains different types of callosal commissural neurons (Voigt *et al.*, 1988; Buhl and Singer, 1989; Martinez-Garcia *et al.*, 1994). They also reported the presence of commissural neurons of pyramidal and non-pyramidal types. Cortical

commissural neurons project to different layers of the contralateral hemisphere (Wise and Jones, 1976; Martinez-Garcia *et al.*, 1994). In so doing, the different types of frontocentral commissural neurons may terminate in different layers of the contralateral hemisphere and may have specific functions in commissural information processing.

## Degeneration of distinct types of commissural neurons in APP23 mice

Two of the three types of commissural neurons were reduced in number when traced in APP23 transgenic mice. Type I commissural neurons were significantly reduced in number in APP23 mice beginning at 5 months of age. The surviving type I commissural neurons in these mice exhibited alterations of the dendritic tree in comparison with wild-type animals. The other types of commissural neurons did not show obvious differences between transgenic and wild-type mouse lines at this point in time. The second type of neurons, type II commissural neurons, was reduced in number at 15 months of age. Thus, the number of traced commissural neurons apparently decreases in APP23-transgenic mice as soon as they start developing Aβ-deposits at 5 months of age. With increasing age, Aβ-plaque load and Aβ-expansion, a second type of neuron becomes involved in Aβ-induced neurodegeneration. However, type III commissural neurons were not altered. The degeneration of type I and II commissural neurons in APP23 mice can be interpreted (i) as a result of selective neuronal death; (ii) as the result of dendritic alterations; or (iii) as a consequence of axonal damage. The first possibility of selective neuronal death is supported by the decrease of the total number of neurons in the hippocampus

of APP-transgenic mice, indicating that neuronal loss can result from abnormal production of Aβ (Calhoun *et al.*, 1998; Schmitz *et al.*, 2004). A second supporting argument is that in Down syndrome patients overexpressing APP (Neve *et al.*, 1988) neuronal loss is accentuated in layer III of the frontocentral cortex (Davidoff, 1928). On the other hand, the second possibility that the reduction of heavily ramified type I commissural neurons is due to dendritic changes is supported by a recent finding indicating that dendritic length is reduced in a specific group of dentate granule cells in PDAPP transgenic mice (Wu *et al.*, 2004). Together with our finding of an asymmetrically ramified dendritic tree in altered type I commissural neurons it is likely that dendritic alterations would at least precede neuronal death. In so doing, it is possible that degenerated type I and II neurons may appear morphologically as type II or III commissural neurons, respectively. The

third hypothesis for the reduction of the number of traced commissural neurons is a loss of axonal connectivity between the hemispheres. This hypothesis is supported by axonal sprouting seen in aged APP-transgenic mice (Phinney *et al.*, 1999; Teter and Ashford, 2002) indicating regeneration after axonal injury (Deller and Jucker, 2001) and by the degeneration of myelinated axons (Bartzokis *et al.*, 2003), especially in the corpus callosum of human Alzheimer's disease cases (Weis *et al.*, 1991; Yamauchi *et al.*, 1993; Hampel *et al.*, 1998). However, our tracing study as well as that of Phinney *et al.* (1999) did not exhibit collateral sprouting of commissural neurons in 5-month-old APP23 mice already exhibiting a decrease in the number of traced type I commissural neurons. Abnormal axonal sprouting of commissural neurons in APP23 mice starts at 11 months of age and, therefore, axonal damage may not be the first step in the degeneration of these neurons.

Single APP and GAP-43 positive neurites occur in the frontocentral cortex of APP23 mice at 5 months, indicative for axonal sprouting (Masliah *et al.*, 1992*a*, *b*). Since commissural neurons do not show sprouting at this age, these APP and GAP-43 positive neurites represent sprouting axon terminals from non-commissural neurons. Such a sprouting is not seen in wild-type littermates. Aβ-aggregates alone do not explain this selective sprouting. If Aβ-aggregates alone would induce such a sprouting, one would expect a contribution of neurites from all types of afferent neurons including commissural neurons. Therefore, it is tempting to speculate that these sprouting neurites in 5-month-old APP23 mice represent reactive sprouting following the degeneration of type I commissural neurons.

Taken together, dendritic and axonal degeneration as well as neuronal death may be involved in the degeneration of type
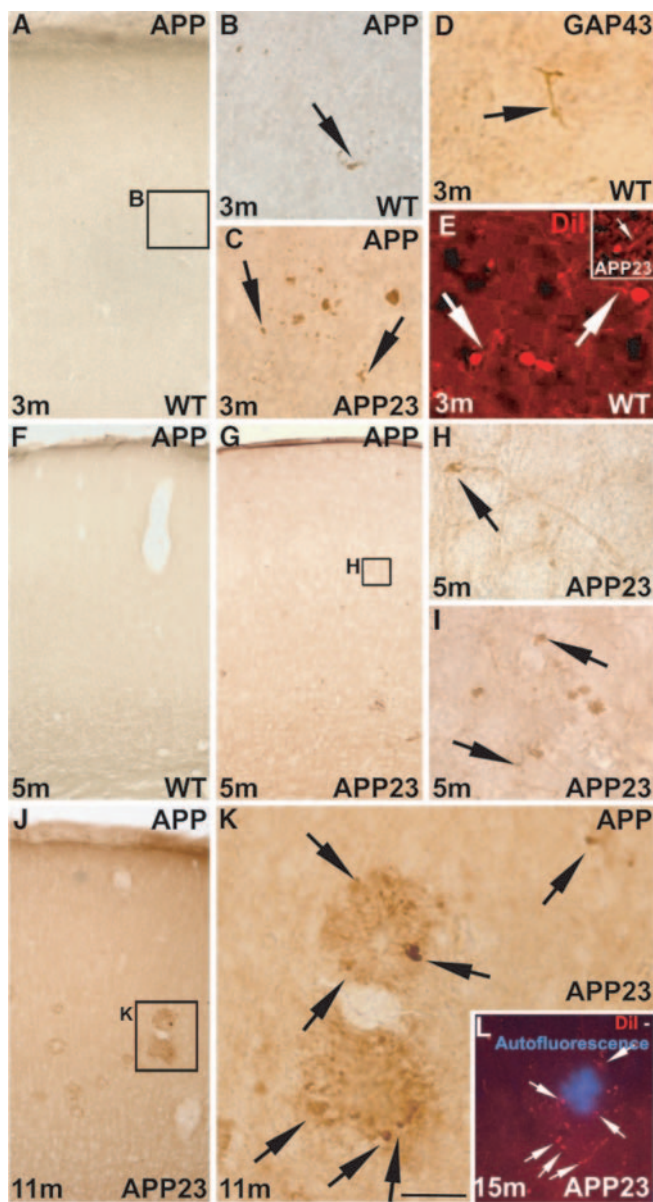
Fig. 7 Sprouting and degenerating axons in the frontocentral cortex of wild-type (wt) and APP23 mice. (**A–E**) APP and GAP43-positive thickened axonal endings in the frontocentral neocortex of wild-type and APP23 mice at 3 months of age. APP positive axonal endings (arrow in **B**) are found in layer III of the frontocentral cortex (**A**, **B** representing the enlargement of the boxed area in **A**). The axonal endings occur in wild-type as well as in APP23 mice and appear as thickened growth cones of sprouting axons (arrows in **B** and **C**) also exhibiting GAP43 (arrow in **D**). DiI tracing also shows swollen axon endings (arrows) in layer III of the contralateral hemisphere indicating an involvement of commissural neurons in these changes (**E**). (**F–I**) At 5 months of age wild-type mice do not show APP or GAP43-positive sprouting or degenerating axons (**F**). In contrast, APP23 mice exhibit single APP-positive, thickened axonal endings (arrows in **H–I**; H represents the enlargement of the boxed area in **G**). (**J–L**) At 11 and 15 months of age APP-positive dystrophic neurites are seen in association with plaques (arrows in **K** representing the enlargement of the boxed area in **J**). Some of these neurites were identified as aberrant sprouting axons (arrows) arising from commissural neurons by DiI tracing around amyloid plaques in the contralateral frontocentral cortex (**L**). The amyloid nature of the plaque is demonstrated by the exhibition of the Aβ-plaque-specific blue autofluorescence under UV-light excitation (Thal *et al.*, 2002*a*). Calibration bar: **A**, **F**, **G** and **J** = 300 μm, **B–E**, **H** and **I** = 20 μm, **K** = 40 μm, **L** = 70 μm.

I and II commissural neurons in a distinct sequence. In a first step dendritic processes of the nerve cells may degenerate presumably followed by axonal damage and, finally, nerve cell death. This sequence is similar to that seen in human Alzheimer's disease for neurons accumulating NFTs (Bancher *et al.*, 1989; Braak *et al.*, 1994; Thal *et al.*, 2000*a*). Here, neurodegeneration starts with dendritic and perikaryal accumulation of abnormal τ-protein, followed by the creation of NFTs, axonal accumulation of abnormal τ-protein in the target region of affected neurons and, finally, neuronal death (Braak *et al.*, 1994; Sassin *et al.*, 2000; Thal *et al.*, 2000*a*).

The relationship between neurodegeneration and Aβ-pathology

The loss of traceable type I commissural neurons in 5-month-old APP23 mice is associated with the deposition of the first Aβ-plaques within the frontal cortex of these animals. However, total Aβ-levels as well as the Aβ-plaque load do not differ significantly between 3- and 5-month-old APP23 mice, and there is no close spatial relationship between Aβ-plaques and degenerating commissural neurons in 5-month-old APP23 mice. These results indicate that Aβ-induced degeneration of neurons in the brain is not due to a simple increase in Aβ-levels or to Aβ-plaques themselves but due to qualitative changes in the status of Aβ-aggregation. Our results support other studies showing that the aggregation of Aβ to soluble Aβ-oligomers and/or fibrils is required for Aβ-toxicity (Podlisny *et al.*, 1995; Kayed *et al.*, 2003; Kim *et al.*, 2003; Cleary *et al.*, 2005) and go beyond the findings of other authors that Aβ-plaques induce local dendritic or neuritic degeneration (Tsai *et al.*, 2004; Brendza *et al.*, 2005; Spires *et al.*, 2005).

Our finding of a hierarchical involvement of different types of neurons in Aβ-induced neurodegeneration further extends the present knowledge of Aβ-toxicity and argues in favour of a selective vulnerability of neurons to Aβ. Since we have studied only commissural neurons projecting into the same area of the contralateral cortex, all neurons have the same axon lengths and all neurons function as commissural neurons. Axon lengths and the function of the neuron do, therefore, not appear to be responsible for the selective vulnerability of distinct types of neurons. All pyramidal neurons use excitatory amino acids (glutamate or aspartate) as transmitter (Conti *et al.*, 1988; Giuffrida and Rustioni, 1989). Thus, at least type I and II commissural neurons share a similar neurotransmitter but differ in their vulnerability. Therefore, the selective vulnerability of commissural neurons is most likely not due to the neurotransmitter of the different types of commissural neurons examined in this study.

The most significant difference between type I, II and III commissural neurons is the morphology of the dendritic tree (Fig. 8). Type I neurons exhibit a highly ramified dendritic tree with basal dendrites branching exclusively in layer III, whereas type II neurons have a less ramified dendritic tree with dendrites also branching into layer IV. The type III neurons, in contrast, show only single dendrites without significant further ramification into secondary and tertiary dendrites. Thus, it is tempting to speculate that neurons with a highly ramified dendritic tree present a better target for toxic changes by oligomeric and/or fibrillar Aβ than neurons with a less ramified dendritic tree. This hypothesis is supported (i) by the finding of Roselli *et al.* (2005) that soluble Aβ-oligomers induce *N*-methyl-D-aspartate (NMDA) dependent degradation of post-synaptic density-95 at glutamatergic synapses on dendrites; (ii) by the Aβ-induced inhibition of long-term potentiation (Wang *et al.*, 2002); and (iii) by the loss of dendritic spines seen in the vicinity of amyloid plaques (Tsai *et al.*, 2004; Spires *et al.*, 2005). Our finding that Aβ-induced neurotoxicity induces dendritic alterations of type I commissural neurons also argues in favour of the dendritic tree to be the primary target of Aβ-toxicity. The primary deposition of Aβ in the neocortical layers III and V (Braak and Braak, 1991; Price *et al.*, 1991; Arriagada *et al.*, 1992; Thal *et al.*, 2000*b*) may support this hypothesis insofar as neurons with a dendritic tree branching exclusively within layer III and the molecular layer are target of Aβ-induced neurodegeneration at an earlier time point compared with neurons with basal dendrites escaping layer III-Aβ by branching into layer IV.

Our results in concert with that of other authors (Wang *et al.*, 2002; Roselli *et al.*, 2005) support the hypothesis that oligomeric and/or fibrillar Aβ-aggregates interact with dendrites and that neurons may degenerate when their dendrites are exposed to Aβ-aggregates. The size of the target for Aβ, that is, the dendritic tree surface in a given area, presumably contributes to the vulnerability of neurons to Aβ. The primary involvement of dendrites in Aβ-toxicity has been demonstrated in dentate gyrus neurons as well (Wu *et al.*, 2004). The interaction of Aβ-oligomeric diffusible ligands (ADDLs) with the dendrites (Lacor *et al.*, 2004) could explain why Wu *et al.* (2004) did not detect any Aβ-deposits although they found dendritic degeneration and it could also explain why 33% of the 5-month-old APP23 mice in our study did show neurodegeneration in the absence of Aβ-deposits. Moreover, it is highly unlikely that the principal function of a neuron (e.g. the function as a commissural neuron), the length of its axon and the neurotransmitter used are the only factors determining selective vulnerability against Aβ. Our results show that theories of selective vulnerability in Alzheimer's disease based upon the principal function and axon length of neurons (Braak *et al.*, 2000) need to be supplemented by other factors to explain Aβ-induced selective vulnerability. The morphology of the dendritic arbor presumably contributes to this selective vulnerability of neurons against Aβ as demonstrated here.

The impact of Aβ-induced progressive neurodegeneration in Alzheimer's disease

In this study we demonstrate that Aβ alters different types of neurons in a distinct hierarchical sequence in an animal
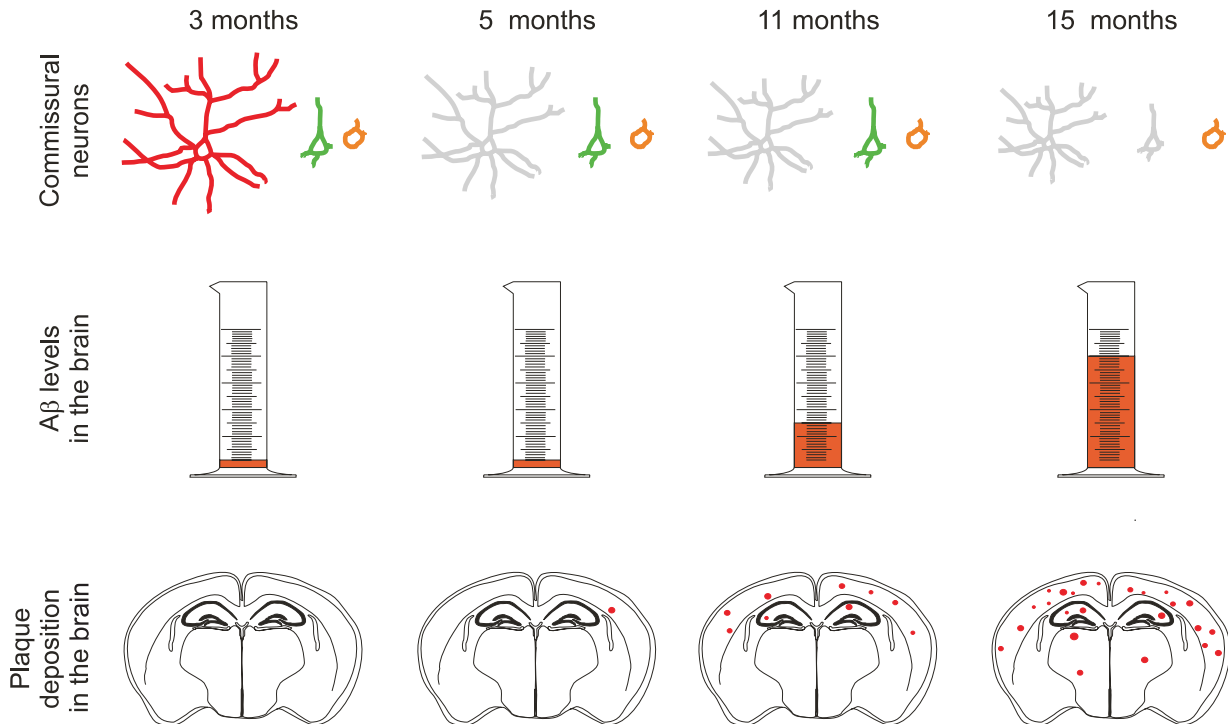
Fig. 8 Neurodegeneration in APP23 mice begins when Aβ-aggregates can be detected as plaques for the first time at 5 months of age. Degeneration of neurons is represented in the figure by changing the colour of the neurons to grey. The Aβ-level in the brain is not responsible for neurodegeneration because 3- and 5-month-old APP23 mice have similar Aβ-levels but only mice at 5 months of age show neurodegeneration. There is selective vulnerability to Aβ-induced neurodegeneration of distinct types of commissural neurons. The type I commissural neurons (red) are most vulnerable to Aβ, whereas type III neurons (orange) are not vulnerable and type II neurons (green) are significantly less vulnerable than type I neurons. The selective vulnerability to Aβ is related to the anatomy of the dendritic tree. Those neurons with the most ramified dendritic tree (type I commissural neurons marked in red) degenerate first. Those neurons with an almost negligible dendritic tree (type III commissural neurons marked in orange) do not degenerate while neurons with a moderately ramified dendritic tree (type II commissural neurons marked in green) degenerate when high levels of Aβ are present in the brain.

model for Aβ-pathology. After onset of degeneration of a distinct type of neurons a further type of neurons became involved with increasing Aβ-pathology. Other studies showing degeneration of different types of neurons in animal models for Alzheimer's disease used double or triple transgenic mice (Lewis *et al.*, 2001; Oddo *et al.*, 2003; Schmitz *et al.*, 2004). In these animals neurodegeneration cannot be addressed exclusively to Aβ because presenilin 1 (Oddo *et al.*, 2003; Schmitz *et al.*, 2004) and/or mutant τ-protein (Lewis *et al.*, 2001; Oddo *et al.*, 2003) are co-expressed. In contrast, single APP-transgenic mice used in this study allow the conclusion that Aβ alone is capable of inducing progressive neurodegeneration. Since humans show a hierarchical sequence in which different types of neurons develop Alzheimer's disease-related NFTs and neuronal loss (Braak and Braak, 1991) that parallels the step-by-step expansion of Aβ-deposits into further brain regions (Thal *et al.*, 2002*b*) similar to neurodegeneration and Aβ-deposition in mice, our present results suggest that Aβ

is capable of inducing progressive neurodegeneration in Alzheimer's disease. Therefore, our results support Aβ to be a major therapeutic target for treatment of Aβ-induced neurodegeneration preferentially in pre-clinical sages. However, since Aβ supports progression of neurodegeneration, Aβ-lowering treatment strategies may also be helpful in later stages to stop the disease progression.

References

Alzheimer A. Ueber eine eigenartige Erkrankung der Hirnrinde. Allg Zschr Psych 1907; 64: 146–8.

Arriagada PV, Marzloff K, Hyman BT. Distribution of Alzheimer-type pathologic changes in nondemented elderly individuals matches the pattern in Alzheimer's disease. Neurology 1992; 42: 1681–8.

Bancher C, Brunner C, Lassmann H, Budka H, Jellinger K, Seitelberger F, et al. Tau and ubiquitin immunoreactivity at different stages of formation of Alzheimer neurofibrillary tangles. Prog Clin Biol Res 1989; 317: 837–48.

Bartzokis G, Cummings JL, Sultzer D, Henderson VW, Nuechterlein KH, Mintz J. White matter structural integrity in healthy aging adults and patients with Alzheimer disease: a magnetic resonance imaging study. Arch Neurol 2003; 60: 393–8.

Bertram L, Tanzi R. Genetics of Alzheimer's disease. In: Dickson D, editor. Neurodegeneration: the molecular pathology of dementia. Basel: ISN Neuropath Press; 2003. p. 40–6.

Braak H, Braak E. Neuropathological staging of Alzheimer-related changes. Acta Neuropathol 1991; 82: 239–59.

Braak E, Braak H, Mandelkow EM. A sequence of cytoskeleton changes related to the formation of neurofibrillary tangles and neuropil threads. Acta Neuropathol 1994; 87: 554–67.

Braak H, Del Tredici K, Schultz C, Braak E. Vulnerability of select neuronal types to Alzheimer's disease. Ann N Y Acad Sci 2000; 924: 53–61.

Brendza RP, Bacskai BJ, Cirrito JR, Simmons KA, Skoch JM, Klunk WE, et al. Anti-Abeta antibody treatment promotes the rapid recovery of amyloid-associated neuritic dystrophy in PDAPP transgenic mice. J Clin Invest 2005; 115: 428–33.

Buhl EH, Singer W. The callosal projection in cat visual cortex as revealed by a combination of retrograde tracing and intracellular injection. Exp Brain Res 1989; 75: 470–6.

Calhoun ME, Wiederhold KH, Abramowski D, Phinney AL, Probst A, Sturchler-Pierrat C, et al. Neuron loss in APP transgenic mice. Nature 1998; 395: 755–6.

Cleary JP, Walsh DM, Hofmeister JJ, Shankar GM, Kuskowski MA, Selkoe DJ, et al. Natural oligomers of the amyloid-beta protein specifically disrupt cognitive function. Nat Neurosci 2005; 8: 79–84.

Conti F, Fabri M, Manzoni T. Glutamate-positive corticocortical neurons in the somatic sensory areas I and II of cats. J Neurosci 1988; 8: 2948–60.

Davidoff LM. The brain in Mongolian idiocy: report of 10 cases. Arch Neurol Psychiatry 1928; 20: 1229–57.

DeKosky ST, Scheff SW. Synapse loss in frontal cortex biopsies in Alzheimer's disease: correlation with cognitive severity. Ann Neurol 1990; 27: 457–64.

Deller T, Jucker M. Axonsrossung im Zentralnervensystem nach einer Läsion. Neuroforum 2001: 11–20.

Dickson DW. The pathogenesis of senile plaques. J Neuropathol Exp Neurol 1997; 56: 321–39.

Duyckaerts C, Dickson DW. Neuropathology of Alzheimer's disease. In: Dickson D, editor. Neurodegeneration: the molecular pathology of dementia and movement disorders. Basel: ISN Neuropath Press; 2003. p. 47–65.

Esiri MM, Hyman BT, Beyreuther K, Masters CL. Ageing and dementia. In: Graham DI, Lantos PL, editors. Greenfield's neuropathology. 6th edn. Vol. 2. London: Arnold; 1997. p. 153–233.

Fritzsch B, Farinas I, Reichardt LF. Lack of neurotrophin 3 causes losses of both classes of spiral ganglion neurons in the cochlea in a region-specific fashion. J Neurosci 1997; 17: 6213–25.

Galuske RA, Singer W. The origin and topography of long-range intrinsic projections in cat visual cortex: a developmental study. Cereb Cortex 1996; 6: 417–30.

Galuske RA, Schlote W, Bratzke H, Singer W. Interhemispheric asymmetries of the modular structure in human temporal cortex. Science 2000; 289: 1946–9.

Games D, Adams D, Alessandrini R, Barbour R, Berthelette P, Blackwell C, et al. Alzheimer-type neuropathology in transgenic mice overexpressing V717F beta-amyloid precursor protein. Nature 1995; 373: 523–7.

Giuffrida R, Rustioni A. Glutamate and aspartate immunoreactivity in cortico-cortical neurons of the sensorimotor cortex of rats. Exp Brain Res 1989; 74: 41–6.

Hampel H, Teipel SJ, Alexander GE, Horwitz B, Teichberg D, Schapiro MB, et al. Corpus callosum atrophy is a possible indicator of region- and cell type-specific neuronal degeneration in Alzheimer disease: a magnetic resonance imaging analysis. Arch Neurol 1998; 55: 193–8.

Hsiao K, Chapman P, Nilsen S, Eckman C, Harigaya Y, Younkin S, et al. Correlative memory deficits, Abeta elevation, and amyloid plaques in transgenic mice. Science 1996; 274: 99–102.

Hsu SM, Raine L, Fanger H. Use of avidin-biotin-peroxidase complex (ABC) in immunoperoxidase techniques: a comparison between ABC and unlabeled antibody (PAP) procedures. J Histochem Cytochem 1981; 29: 577–80.

Hughes CM, Peters A. Types of callosally projecting nonpyramidal neurons in rat visual cortex identified by lysosomal HRP retrograde labeling. Anat Embryol (Berl) 1992; 186: 183–93.

Kang J, Lemaire HG, Unterbeck A, Salbaum JM, Masters CL, Grzeschik KH, et al. The precursor of Alzheimer's disease amyloid A4 protein resembles a cell-surface receptor. Nature 1987; 325: 733–6.

Kayed R, Head E, Thompson JL, McIntire TM, Milton SC, Cotman CW, et al. Common structure of soluble amyloid oligomers implies common mechanism of pathogenesis. Science 2003; 300: 486–9.

Kim HJ, Chae SC, Lee DK, Chromy B, Lee SC, Park YC, et al. Selective neuronal degeneration induced by soluble oligomeric amyloid beta protein. FASEB J 2003; 17: 118–20.

Klafki HW, Wiltfang J, Staufenbiel M. Electrophoretic separation of betaA4 peptides (1-40) and (1-42). Anal Biochem 1996; 237: 24–9.

Lacor PN, Buniel MC, Chang I, Fernandez SJ, Gong Y, Viola KL, et al. Synaptic targeting by Alzheimer's-related amyloid beta oligomers. J Neurosci 2004; 24: 10191–200.

Lewis J, Dickson DW, Lin WL, Chisholm L, Corral A, Jones G, et al. Enhanced neurofibrillary degeneration in transgenic mice expressing mutant tau and APP. Science 2001; 293: 1487–91.

Martinez-Garcia F, Gonzalez-Hernandez T, Martinez-Millan L. Pyramidal and nonpyramidal callosal cells in the striate cortex of the adult rat. J Comp Neurol 1994; 350: 439–51.

Masliah E, Mallory M, Ge N, Saitoh T. Amyloid precursor protein is localized in growing neurites of neonatal rat brain. Brain Res 1992a; 593: 323–8.

Masliah E, Mallory M, Hansen L, Alford M, DeTeresa R, Terry R, et al. Localization of amyloid precursor protein in GAP43-immunoreactive aberrant sprouting neurites in Alzheimer's disease. Brain Res 1992b; 574: 312–6.

Masliah E, Mallory M, Hansen L, DeTeresa R, Alford M, Terry R. Synaptic and neuritic alterations during the progression of Alzheimer's disease. Neurosci Lett 1994; 174: 67–72.

Masliah E, Sisk A, Mallory M, Mucke L, Schenk D, Games D. Comparison of neurodegenerative pathology in transgenic mice overexpressing V717F beta-amyloid precursor protein and Alzheimer's disease. J Neurosci 1996; 16: 5795–811.

Masters CL, Multhaup G, Simms G, Pottgiesser J, Martins RN, Beyreuther K. Neuronal origin of a cerebral amyloid: neurofibrillary tangles of Alzheimer's disease contain the same protein as the amyloid of plaque cores and blood vessels. EMBO J 1985; 4: 2757–63.

Neve RL, Finch EA, Dawes LR. Expression of the Alzheimer amyloid precursor gene transcripts in the human brain. Neuron 1988; 1: 669–77.

Oddo S, Caccamo A, Shepherd JD, Murphy MP, Golde TE, Kayed R, et al. Triple-transgenic model of Alzheimer's disease with plaques and tangles: intracellular Abeta and synaptic dysfunction. Neuron 2003; 39: 409–21.

Phinney AL, Deller T, Stalder M, Calhoun ME, Frotscher M, Sommer B, et al. Cerebral amyloid induces aberrant axonal sprouting and ectopic terminal formation in amyloid precursor protein transgenic mice. J Neurosci 1999; 19: 8552–9.

Podlisny MB, Ostaszewski BL, Squazzo SL, Koo EH, Rydell RE, Teplow DB, et al. Aggregation of secreted amyloid beta-protein into sodium dodecyl sulfate-stable oligomers in cell culture. J Biol Chem 1995; 270: 9564–70.

Price JL, Davis PB, Morris JC, White DL. The distribution of tangles, plaques and related immunohistochemical markers in healthy aging and Alzheimer's disease. Neurobiol Aging 1991; 12: 295–312.

Reiner A, Veenman CL, Medina L, Jiao Y, Del Mar N, Honig MG. Pathway tracing using biotinylated dextran amines. J Neurosci Methods 2000; 103: 23–37.

Roselli F, Tirard M, Lu J, Hutzler P, Lamberti P, Livrea P, et al. Soluble beta-amyloid1-40 induces NMDA-dependent degradation of postsynaptic density-95 at glutamatergic synapses. J Neurosci 2005; 25: 11061–70.

Sassin I, Schultz C, Thal DR, Rub U, Arai K, Braak E, et al. Evolution of Alzheimer's disease-related cytoskeletal changes in the basal nucleus of Meynert. Acta Neuropathol (Berl) 2000; 100: 259–69.

Schmitz C, Rutten BP, Pielen A, Schafer S, Wirths O, Tremp G, et al. Hippocampal neuron loss exceeds amyloid plaque load in a transgenic mouse model of Alzheimer's disease. Am J Pathol 2004; 164: 1495–502.

Schrader-Fischer G, Paganetti PA. Effect of alkalizing agents on the processing of the beta-amyloid precursor protein. Brain Res 1996; 716: 91–100.

Spires TL, Meyer-Luehmann M, Stern EA, McLean PJ, Skoch J, Nguyen PT, et al. Dendritic spine abnormalities in amyloid precursor protein transgenic mice demonstrated by gene transfer and intravital multiphoton microscopy. J Neurosci 2005; 25: 7278–87.

Staufenbiel M, Paganetti PA. Electrophoretic separation and immunoblotting of Aβ1-40 and Aβ1-42. In: Methods in molecular medicine: Alzheimer's disease: methods and protocols. Vol. 32. Totowa, NJ: Humana Press, 1999; p. 91–99.

Sturchler-Pierrat C, Abramowski D, Duke M, Wiederhold KH, Mistl C, Rothacher S, et al. Two amyloid precursor protein transgenic mouse models with Alzheimer disease-like pathology. Proc Natl Acad Sci USA 1997; 94: 13287–92.

Tanzi RE, Gusella JF, Watkins PC, Bruns GA, St George-Hyslop P, Van Keuren ML, et al. Amyloid beta protein gene: cDNA, mRNA distribution, and genetic linkage near the Alzheimer locus. Science 1987; 235: 880–4.

Terry RD, Peck A, DeTeresa R, Schechter R, Horoupian DS. Some morphometric aspects of the brain in senile dementia of the Alzheimer type. Ann Neurol 1981; 10: 184–92.

Teter B, Ashford JW. Neuroplasticity in Alzheimer's disease. J Neurosci Res 2002; 70: 402–37.

Thal DR, Holzer M, Rüb U, Waldmann G, Gunzel S, Zedlick D, et al. Alzheimer-related tau-pathology in the perforant path target zone and in the hippocampal stratum oriens and radiatum correlates with onset and degree of dementia. Exp Neurol 2000a; 163: 98–110.

Thal DR, Rüb U, Schultz C, Sassin I, Ghebremedhin E, Del Tredici K, et al. Sequence of Abeta-protein deposition in the human medial temporal lobe. J Neuropathol Exp Neurol 2000b; 59: 733–48.

Thal DR, Ghebremedhin E, Haass C, Schultz C. UV light-induced autofluorescence of full-length Abeta-protein deposits in the human brain. Clin Neuropathol 2002a; 21: 35–40.

Thal DR, Rüb U, Orantes M, Braak H. Phases of Abeta-deposition in the human brain and its relevance for the development of AD. Neurology 2002b; 58: 1791–1800.

Thal DR, Capetillo-Zarate E, Del Tredici K, Braak H. The development of amyloid β-protein (Aβ)-deposits in the aged brain. Sci Aging Knowl Environ 2006; 6, re1.

Tsai J, Grutzendler J, Duff K, Gan WB. Fibrillar amyloid deposition leads to local synaptic abnormalities and breakage of neuronal branches. Nat Neurosci 2004; 7: 1181–3.

Voigt T, LeVay S, Stamnes MA. Morphological and immunocytochemical observations on the visual callosal projections in the cat. J Comp Neurol 1988; 272: 450–60.

Wang HW, Pasternak JF, Kuo H, Ristic H, Lambert MP, Chromy B, et al. Soluble oligomers of beta amyloid (1-42) inhibit long-term potentiation but not long-term depression in rat dentate gyrus. Brain Res 2002; 924: 133–40.

Weis S, Jellinger K, Wenger E. Morphometry of the corpus callosum in normal aging and Alzheimer's disease. J Neural Transm Suppl 1991; 33: 35–8.

Wiederhold K-H, Staufenbiel M, Mistl C, Danner S. Stages of amyloid deposition and plaque types in different APP transgenic mice as compared to AD [abstract]. Neurobiol Aging 2004; 25 (Suppl. 2): 254–5.

Wild-Bode C, Yamazaki T, Capell A, Leimer U, Steiner H, Ihara Y, et al. Intracellular generation and accumulation of amyloid beta-peptide terminating at amino acid 42. J Biol Chem 1997; 272: 16085–8.

Wise SP, Jones EG. The organization and postnatal development of the commissural projection of the rat somatic sensory cortex. J Comp Neurol 1976; 168: 313–43.

Wu CC, Chawla F, Games D, Rydel RE, Freedman S, Schenk D, et al. Selective vulnerability of dentate granule cells prior to amyloid deposition in PDAPP mice: digital morphometric analyses. Proc Natl Acad Sci USA 2004; 101: 7141–6.

Yamauchi H, Fukuyama H, Harada K, Nabatame H, Ogawa M, Ouchi Y, et al. Callosal atrophy parallels decreased cortical oxygen metabolism and neuropsychological impairment in Alzheimer's disease. Arch Neurol 1993; 50: 1070–4.

Yamaguchi H, Sugihara S, Ogawa A, Saido TC, Ihara Y. Diffuse plaques associated with astroglial amyloid beta protein, possibly showing a disappearing stage of senile plaques. Acta Neuropathol (Berl) 1998; 95: 217–22.